

PHANGS-JWST First Results: Destruction of the PAH molecules in HII regions probed by JWST and MUSE

OLEG V. EGOROV ¹, KATHRYN KRECKEL ¹, KARIN M. SANDSTROM ², ADAM K. LEROY ³, SIMON C. O. GLOVER ⁴, BRENT GROVES ⁵, J. M. DIEDERIK KRUIJSSEN ⁶, ASHLEY. T. BARNES ⁷, FRANCESCO BELFIORE ⁸, F. BIGIEL ⁷, GUILLERMO A. BLANC ^{9,10}, MÉDÉRIC BOQUIEN ¹¹, YIXIAN CAO ¹², JÉRÉMY CHASTENET ¹³, MÉLANIE CHEVANCE ^{4,6}, ENRICO CONGIU ¹⁰, DANIEL A. DALE ¹⁴, ERIC EMSELLEM ^{15,16}, KATHRYN GRASHA ¹⁷, RALF S. KLESSEN ^{4,18}, KIRSTEN L. LARSON ¹⁹, DAIZHONG LIU ¹², ERIC J. MURPHY ²⁰, HSI-AN PAN ²¹, ISMAEL PESSA ²², JÉRÔME PETY ^{23,24}, ERIK ROSOLOWSKY ²⁵, FABIAN SCHEUERMANN ¹, EVA SCHINNERER ²², JESSICA SUTTER ^{2,26}, DAVID A. THILKER ²⁷, ELIZABETH J. WATKINS ¹ AND THOMAS G. WILLIAMS ^{28,22}

ABSTRACT

Polycyclic aromatic hydrocarbons (PAHs) play a critical role in the reprocessing of stellar radiation and in balancing the heating and cooling processes in the interstellar medium (ISM), but appear to be destroyed in H II regions. However, the mechanisms driving their destruction are still not completely understood. Using PHANGS-JWST and PHANGS-MUSE observations, we investigate how the PAH fraction changes in about 1500 H II regions across four nearby star-forming galaxies (NGC 628, NGC 1365, NGC 7496, IC 5332). We find a strong anti-correlation between the PAH fraction and the ionization parameter (the ratio between the ionizing photon flux and the hydrogen density) of H II regions. This relation becomes steeper for more luminous H II regions. The metallicity of H II regions has only a minor impact on these results in our galaxy sample. We find that the PAH fraction decreases with the H α equivalent width – a proxy for the age of the H II regions – although this trend is much weaker than the one identified using the ionization parameter. Our results are consistent with a scenario where hydrogen-ionizing UV radiation is the dominant source of PAH destruction in star-forming regions.

Keywords: Interstellar dust (836) — H II regions (694) — Polycyclic aromatic hydrocarbons (1280)

1. INTRODUCTION

Polycyclic aromatic hydrocarbons (PAHs) are carbon-based macromolecules that are ubiquitous in the interstellar medium (ISM), and are traced by several strong emission features at 3.3, 6.2, 7.7, 8.6, 11.3, 12.7, and 17 μm (Tielens 2008; Li 2020). Together with very small (20 – 30 Å) dust grains that have been stochastically heated, PAHs can be a dominant contributor to the mid-infrared (mid-IR) spectra of galaxies (e.g. Draine & Li 2007). The IR emission from PAHs is produced by the absorption and re-emission of ultraviolet (UV) photons, with PAHs reprocessing as much as 20% of all stellar UV radiation (Smith et al. 2007). Because of this, they have been proposed as indicators of star formation rate (Calzetti 2013), but their usage for this purpose is

complicated by our lack of understanding of the mechanisms for PAH formation and destruction (Whitcomb et al. 2020).

PAHs are formed in the carbon-rich atmospheres of evolved stars (e.g. Latter 1991; Cherchneff et al. 1992), though these PAHs alone cannot account for all the PAH emission observed in the ISM (e.g. Matsuura et al. 2009, 2013). The precursor molecules for PAHs have been found in dense clouds (Burkhardt et al. 2021), and high PAH fractions are observed in molecular clouds, which is difficult to explain if they do not form there given cloud lifetimes (Sandstrom et al. 2010; Chastenet et al. 2019). A popular scenario for PAH formation is the shattering of larger dust grains (e.g. Jones et al. 1996; Hirashita & Yan 2009; Seok et al. 2014; Wiebe et al. 2014). Both shocks and UV radiation play a critical but complex role in the evolution of PAHs. Shocks can increase the PAH fraction by dissociating large grains, but also decrease the PAH abundance by destroying them

directly (e.g. O’Halloran et al. 2006; Micelotta et al. 2010a). Similarly, UV radiation excites the IR bands in PAHs, but can also destroy them (e.g. Allain et al. 1996; Pavlyuchenkov et al. 2013).

PAH destruction is thought to be regulated by the radiation field, either by the high intensity of ionizing photons (Montillaud et al. 2013) or the hardness¹ of the radiation (Madden et al. 2006; Gordon et al. 2008). Theoretical works also suggest that PAHs are subject to sputtering and fragmentation in ionized gas due to electronic and atomic interactions (Micelotta et al. 2010b; Bocchio et al. 2012). These processes should destroy PAH molecules, and thus reduce their abundance in H II regions. Observationally, this has been seen as a lack of PAH emission in the interior of Galactic H II regions (e.g. Povich et al. 2007), and an anti-correlation between the PAH fraction and tracers of the hardness and/or intensity of the ionizing radiation on large (global) scales (e.g. Madden et al. 2006; Gordon et al. 2008; Hunt et al. 2010; Lebouteiller et al. 2011; Maragkoudakis et al. 2018). Hydrogen-ionizing radiation is often considered a natural explanation for the observed decrease of the PAH abundances in low-metallicity galaxies and star-forming complexes (e.g. Engelbracht et al. 2005; Madden et al. 2006; Engelbracht et al. 2008; Khramtsova et al. 2013).

The properties of star-forming regions (e.g. age, metallicity, density) establish the balance between the PAH formation and destruction processes. Multi-wavelength observations of H II regions, their stellar populations and associated photo-dissociation regions (PDR) are therefore key for understanding the evolution of PAHs in the ISM of galaxies, and high (<100 pc) physical resolutions are critical to spatially isolating local from global effects (see also Chasten et al. *subm.a*). Until now, such observations were possible mainly in H II regions in our Galaxy (e.g. Povich et al. 2007; Binder & Povich 2018), or very nearby galaxies (e.g. Bolatto et al. 2007; Sandstrom et al. 2010; Wiebe et al. 2011; Lebouteiller et al. 2011; Chasten et al. 2017; Maragkoudakis et al. 2018; Chasten et al. 2019; Mallory et al. 2022), while most extragalactic studies were focused on integrated observations of entire galaxies or of large star-forming complexes (e.g. Engelbracht et al. 2005; Madden et al. 2006; Gordon et al. 2008; Khramtsova et al. 2013, 2014; Maragkoudakis et al. 2018; Lin et al. 2020).

With the launch of the *JWST*, it is now possible to investigate individual H II regions and their immedi-

ate surroundings in significantly more distant galaxies than ever before, covering a more representative view of physical conditions in the ISM. Combining new *JWST* data with the available high-resolution data in different wavelength ranges, we can probe now the evolution of the PAHs and other grains in connection with the star-forming H II regions.

In this letter, we explore the abundance of PAH molecules within the boundaries of H II regions at 28–64 pc resolution in four nearby star-forming galaxies observed with *JWST* as the first targets in the PHANGS-*JWST* treasury program (Lee et al. 2022a). We use MIRI images as tracers of emission from PAHs and very small dust grains. We combine these data with optical spectroscopy obtained from the MUSE integral-field spectrograph (Bacon et al. 2010) on the VLT as part of the PHANGS-MUSE program (Emsellem et al. 2022). Based on these data sets, we investigate the relation between the PAH fraction and properties of the H II regions that could be potentially regulating their destruction (or formation). We refer the reader to the accompanying paper by Chasten et al. (*subm.a*), where we analyze the PAH fraction on galaxy-wide scales.

This letter is organized as follows. In Section 2 we describe the underlying observational data. Section 3 provides details on the methods and criteria implemented for selection of the H II regions and deriving the properties of the gas, dust and young stars there. Section 4 describes results from the comparison of our tracer for PAH abundance and properties of the H II regions. Section 5 summarizes our results.

2. OBSERVATIONS

2.1. Galaxy sample

We analyze H II regions in the first four PHANGS-*JWST* galaxies. These galaxies have all been observed with VLT/MUSE, and thus are ideal objects to relate the properties of ionized gas to the PAH emission. These nearby ($D \sim 9\text{--}20$ Mpc) galaxies span an order of magnitude in stellar mass (see Table 1), and almost two orders of magnitude in star formation rate (SFR). Two galaxies (NGC 1365 and NGC 7496) host active galactic nuclei (AGNs) and strong bars. NGC 628 is a prototypical grand-design spiral, while IC 5332 shows a flocculent spiral morphology. They represent a good cross-section of the PHANGS-*JWST* sample (Fig. 1).

2.2. PHANGS-*JWST*

The *JWST* data were obtained in Cycle 1 as part of the PHANGS-*JWST* program (ID 02107; PI: J. C. Lee). The survey targets 19 nearby star-forming galaxies with NIRCcam (F200W, F300M, F335M and F360M) and

¹ Various definitions are used in the literature (e.g., the effective temperature, or the spectral index of the UV spectrum). Here we define ‘hardness’ as the ratio of the fluxes over hard and soft UV ranges (see Appendix A).

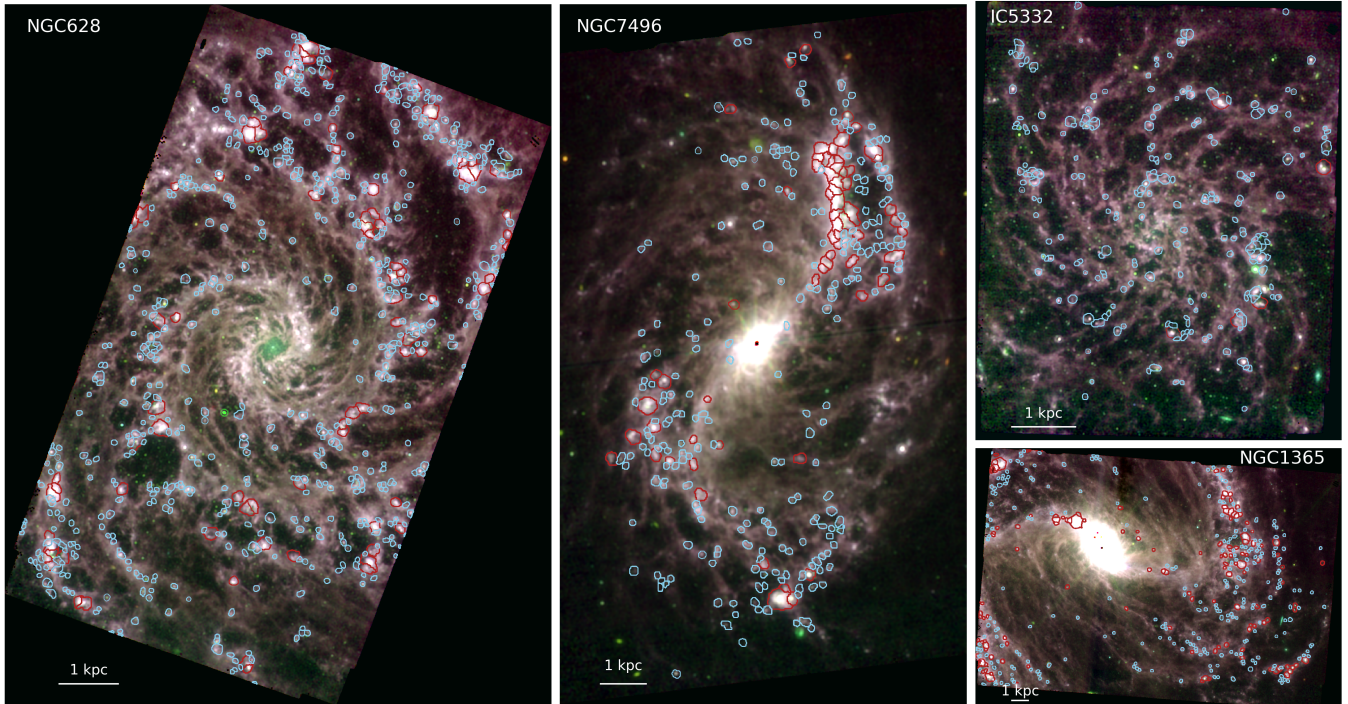


Figure 1. JWST/MIRI images in the F770W, F1000W and F1130W bands (red, green and blue channels, respectively) of the four galaxies analyzed in this letter. Contours show the borders of individual H II regions selected from MUSE data, which meet the criteria in Sec. 3.1. Blue contours correspond to the H II regions with hydrogen-ionizing photons rate $Q^0 < 10^{50} \text{ s}^{-1}$, and red contours to those with $Q^0 > 10^{50} \text{ s}^{-1}$.

Table 1. Properties of the galaxies

Galaxy	D (Mpc)	R_{25}^\dagger (kpc)	$\log M_*^+$ (M_\odot)	$\log(\text{SFR})^+$ ($M_\odot \text{ yr}^{-1}$)	$12+\log(\text{O}/\text{H})^*$ at R_{eff}	N_{HII}
IC5332	9.01 ¹	8.0	9.67	-0.39	8.30	208
NGC628	9.84 ¹	14.1	10.34	0.24	8.48	668
NGC1365	19.57 ¹	34.2	10.99	1.23	8.48	365
NGC7496	18.72 ²	9.1	10.00	0.35	8.51	288

References: [†]Paturel et al. (2003); ⁺Leroy et al. (2021); ^{*}Groves et al, submitted;

¹Anand et al. (2021a,b); ²Anand et al. (2021a); Shaya et al. (2017); Kourkchi et al. (2020)

MIRI (F770W, F1000W, F1130W and F2100W) imaging. The first four galaxies have been observed, and their MIRI images (Fig. 1) form the basis of our analysis. These galaxies have been imaged with two (for IC 5332 and NGC 7496), three (for NGC 628) or four (NGC 1365) MIRI pointings (88.8, 122.1, 310.8, 321.9 seconds per pointing in the F770W, F1000W, F1130W and F2100W bands, respectively, and with 4 dithers per pointing to properly sample the PSF), covering an area well-matched to the PHANGS-MUSE (Emsellem et al. 2022) and PHANGS-HST observations (Lee et al. 2022b). The sensitivity of the data is similar for all four galaxies in all MIRI bands (0.11 – 0.15 MJy sr⁻¹ at 1 σ level) except F2100W ($\sim 0.25 \text{ MJy sr}^{-1}$). We convolve all images to the PSF of the F2100W images

(FWHM $\simeq 0.67''$; corresponding to 28–64 pc at the distance of our targets), as obtained via the WEBBPSF (Perin et al. 2014) model². Convolution kernels were created following the procedure from Aniano et al. (2011). Standard calibrations are applied, with minor modifications. A detailed description of the complete data reduction is presented in Lee et al. (2022a).

2.3. PHANGS-MUSE

All the galaxies in the PHANGS-JWST program were previously observed with VLT/MUSE as part of the PHANGS-MUSE large program (PI: Schinnerer). The

² <https://webbpsf.readthedocs.io/en/stable/index.html>

reduced data are publicly available³, and the details of the observations and data reduction are given in [Emmellem et al. \(2022\)](#). The angular resolution of the MUSE data for the objects in this study is $\sim 1''$ (45–95 pc), sufficient to isolate individual H II regions from surrounding diffuse ionized gas (DIG).

Based on MUSE H α emission line maps, a catalog of $\sim 30,000$ nebulae has been constructed ([Santoro et al. 2022](#), [Groves et al. submitted](#)). The nebulae were selected using HIIPHOT ([Thilker et al. 2000](#)), which results in spatial masks that define the borders of each nebula. The catalog contains derived properties of each nebula (e.g., emission line fluxes, velocity dispersion, equivalent width, metallicity) based on their integrated spectra. The emission lines from each nebula are corrected for the effects of dust extinction using the Balmer decrement, as described in [Groves et al.](#) In the remainder of this paper, we use the extinction-corrected values. We do not correct the measured fluxes for the contribution of the DIG. H II regions are selected from the nebulae catalog based on the [Baldwin et al. \(1981\)](#) diagnostics considering [O III]/H β vs [N II]/H α and [S II]/H α line ratios, as described in [Groves et al. \(submitted\)](#), see also [Kewley et al. 2019](#) for a review). The present analysis is restricted to only those H II regions that meet stringent surface brightness and signal-to-noise (S/N) criteria (see [Sec. 3.1](#)).

3. DERIVING THE PROPERTIES OF THE IONIZED GAS AND PAHs IN STAR-FORMING REGIONS

3.1. Selection of the nebulae and associated PAH emission

We use the spatial masks from the PHANGS-MUSE nebular catalog (see [Sec. 2.3](#)) to identify the positions of H II regions in the *JWST* data. To do that, we reproject these masks to the *JWST* images. Since two of our galaxies contain an AGN, which produces hard ionizing radiation that can significantly affect the PAH fraction (e.g. [Jensen et al. 2017](#); [Lai et al. 2022](#); [García-Bernete et al. 2022](#)), we exclude the centers of the galaxies from our analysis. Masks that isolate these particular environments are taken from [Querejeta et al. \(2021\)](#).

In order to minimize the DIG contribution to the regions’ flux, which could bias derived properties of the nebulae, we select only those H II regions with high H α equivalent width $EW(H\alpha) > 16 \text{ \AA}$ and H α surface brightness $\Sigma(H\alpha) > 10^{39} \text{ erg s}^{-1} \text{ kpc}^{-2}$ (e.g. [Belfiore et al. 2022](#)). We also require $S/N > 5$ in every emis-

sion line considered in this letter, and $S/N > 15$ in the H α line. This ensures that we can recover accurate reddening-corrected fluxes of emission lines and derived properties for each of the nebulae.

In total, we select 1529 H II regions across all four galaxies (N_{HII} in [Tab. 1](#)) – about 25% of the H II regions in our catalog (37% for NGC 1365). We derive the ratio $\log([\text{S III}]\lambda 9069, 9532\text{\AA}/[\text{S II}]\lambda 6717, 6731\text{\AA})^4$, which is a proxy for the ionization parameter (the ratio of the local ionizing photon flux and the local hydrogen density; [Kewley & Dopita 2002](#)), and we measure the oxygen abundance $12 + \log(\text{O}/\text{H})$ (a proxy for gas-phase metallicity) with the S-calibration from [Pilyugin & Grebel \(2016\)](#). We integrate the fluxes in each *JWST* MIRI band within the apertures corresponding to the reprojected mask for each region. Some ratios of these mid-IR fluxes trace the PAH abundance in the ISM. We do not correct the measured fluxes for possible contribution from the diffuse ISM. Note, however, that removing the local background measured in circular apertures around H II regions does not affect qualitatively the results presented below.

3.2. Tracing the PAH fraction in the ISM

The ratio of total fluxes in the *Spitzer* bands $F_{8\mu\text{m}}/F_{24\mu\text{m}}$ is often considered as a tracer of q_{PAH} – the mass fraction of PAH molecules with respect to the total dust mass (e.g. [Engelbracht et al. 2005](#); [Bolatto et al. 2007](#); [Sandstrom et al. 2010](#); [Khrantsova et al. 2014](#); [Oey et al. 2017](#)). [Sandstrom et al. \(2010\)](#) have shown that $F_{8\mu\text{m}}/F_{24\mu\text{m}}$ is indeed a good tracer of q_{PAH} , although it has a large scatter in the diffuse low-metallicity ISM where $q_{\text{PAH}} < 1.5\%$. [Khrantsova et al. \(2013\)](#) found a stronger correlation between these parameters in star-forming regions.

In the case of *JWST*, the flux of the F2100W band traces the emission from very small dust grains (similar to *Spitzer* 24 μm) and correlates with the total IR luminosity (F_{TIR}), whereas F770W and F1130W are dominated by PAH features at 7.7 μm (similar to *Spitzer* 8 μm) and 11.3 μm , respectively, and trace the neutral and ionized ISM ([Sandstrom et al. subm.](#)). Models by [Draine et al. \(2021\)](#) show that q_{PAH} is proportional to both $F_{7.7}/F_{\text{TIR}}$ and $F_{11.2}/F_{\text{TIR}}$. Using $F_{2100\text{W}}$ as a proxy for F_{TIR} introduces an unknown scaling, but provides a robust empirical tracer of q_{PAH} ([Chastenet et al. subm.a](#)). In this letter, we consider both the 7.7 μm and

³ https://archive.eso.org/scienceportal/home?data_collection=PHANGS

⁴ While [S III] $\lambda 9532$ is outside the MUSE spectral range, the two [S III] lines show a fixed ratio, which we assume to be $[\text{S III}]\lambda 9532\text{\AA} \simeq 2.5 \times [\text{S III}]\lambda 9069\text{\AA}$ ([Osterbrock & Ferland 2006](#))

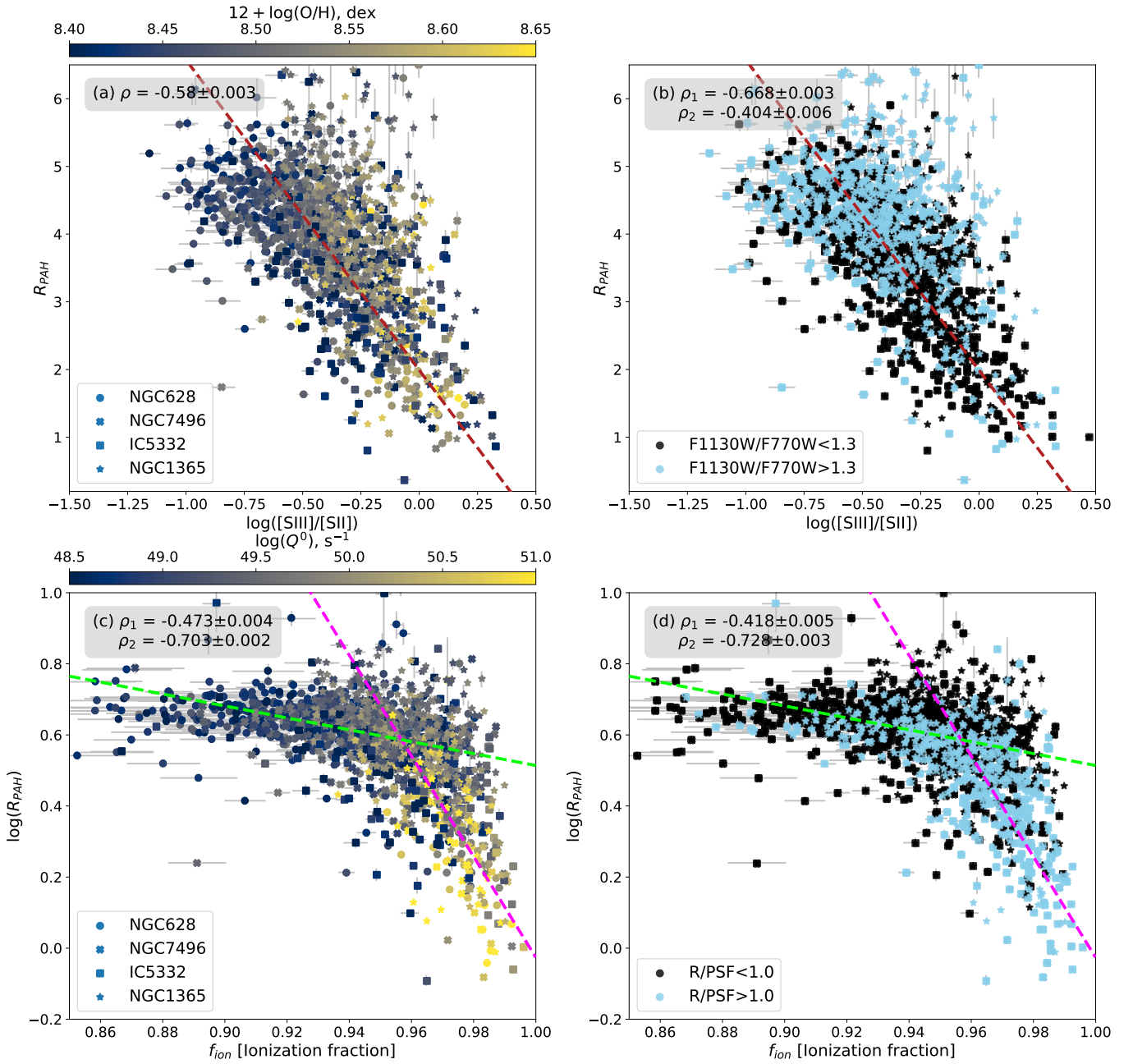


Figure 2. Correlation of PAH abundance, traced by R_{PAH} , with ionization parameter, traced by $\log([\text{S III}]/[\text{S II}])$ (Panels a, b), or ionization fraction f_{ion} (Panels c, d). Color encodes the oxygen abundance $12 + \log(\text{O}/\text{H})$ (Panel a), ratio of F1130W/F770W – a proxy for the ionization state of PAHs (Panel b), number of hydrogen ionizing photons Q^0 (Panel c), and effective radii of the H II regions relative to the PSF of the MUSE data (Panel d). Dashed lines show a linear fit for the H II regions (Eq. 2 for Panels a,b). Faint ($Q^0 < 10^{50} \text{ s}^{-1}$; green dashed line, Eq. 3) and bright ($Q^0 > 10^{50} \text{ s}^{-1}$; magenta dashed line, Eq. 4) H II regions are considered separately on Panels c and d. The Spearman's correlation coefficient (ρ) is given in the corner of each plot. Coefficients ρ_1 and ρ_2 are calculated separately for the black and cyan points (Panels b and d), or for the faint and bright regions (Panel c), respectively. The errors on ρ are derived from 1000 Monte Carlo realization with the data randomly distributed around the measured values within the uncertainties.

11.3 μm PAH features and assume that:

$$q_{\text{PAH}} \propto R_{\text{PAH}} = \frac{F_{F770W} + F_{F1130W}}{F_{F2100W}}. \quad (1)$$

Similarly to the works mentioned above, we assume further that R_{PAH} changes in H II regions mostly due to variations of the PAH fraction regulated by the processes of their formation and destruction. Note, however, that redistribution of the dust grains of different sizes can also affect R_{PAH} if the relative abundance of very small grains is changing in H II regions. For example, [Everett & Churchwell \(2010\)](#) hypothesized that the very small grains could be re-supplied by the destruction of the dense embedded cloudlets overrun by the expansion of a bubble. Furthermore, radiation-pressure-driven shift or/and the stellar winds ([Gail & Sedlmayr 1979](#); [Draine 2011](#)) can redistribute the PAHs and very small grains, which has been suggested as a mechanism for evacuating the dust grains from the interior of several Galactic H II regions ([Paladini et al. 2012](#)). Shell-like morphology of the Galactic H II regions is indeed clearly seen in the mid-IR bands, especially in PAH-sensitive bands (e.g. [Anderson et al. 2014](#)). However, small grains ($< 100 \text{ \AA}$) drift much more slowly than larger grains, and the difference between the PAHs and the very small grains is insignificant ([Draine 2011](#)). Thus, these processes should not significantly change the relative fraction of PAHs within the H II regions. Nevertheless, both of these effects can change the relative brightness of the rims of the H II regions in the mid-IR bands. Given that we analyze the ratios of the fluxes integrated over the H II regions, excluding the surrounding PDR (at least for the resolved H II regions, see [Sec. 4.1](#)), our results presented below are unlikely to be affected by these processes.

4. RESULTS AND DISCUSSION

4.1. Destruction of PAHs by UV radiation

PAH destruction is expected to be correlated with the hardness and intensity of the radiation field (see [Sec. 1](#)). In previous works (e.g. [Madden et al. 2006](#); [Gordon et al. 2008](#); [Lebouteiller et al. 2011](#); [Maragkoudakis et al. 2018](#)), the flux ratio of the neon IR lines $[\text{Ne III}]15.56 \mu\text{m}/[\text{Ne II}]12.81 \mu\text{m}$ was used as a tracer of the hardness of the ionizing radiation field. As shown in [Kewley et al. \(2019\)](#), this ratio is dependent on both the ionization parameter and the metallicity. In turn, the hardness of the radiation field depends on the metallicity (e.g. [Groves et al. 2008](#)), and can be correlated with the ionization parameter in H II regions (see discussion in [Kumari et al. 2021](#)). In this work, we use another tracer of the ionization parameter – $[\text{S III}]\lambda 9069,9532\text{\AA}/[\text{S II}]\lambda 6717,6731\text{\AA}$, which

can be measured in optical spectra. In contrast to $[\text{Ne III}]/[\text{Ne II}]$, this ratio of sulfur lines is almost independent of metallicity ([Kewley et al. 2019](#)) and thus allows us to explore the relation of PAH abundances with the properties of the ionizing radiation field and the metallicity separately.

In [Fig. 2\(a, b\)](#) we demonstrate how R_{PAH} depends on $\log([\text{S III}]/[\text{S II}])$ in the 1529 H II regions. The data shows a strong anti-correlation, implying that the PAH fraction in H II regions is tightly related to the ionization parameter. This anti-correlation can be parameterized linearly as:

$$R_{\text{PAH}} = (-4.58 \pm 0.16) \times \log([\text{S III}]/[\text{S II}]) + (1.99 \pm 0.06) + \Delta R_{\text{O/H}}, \quad (2)$$

where $\Delta R_{\text{O/H}}$ accounts for any secondary dependence on metallicity. For now, we assume $\Delta R_{\text{O/H}} = 0$ as we do not see a significant secondary correlation of R_{PAH} with $12 + \log(\text{O/H})$ in [Panel \(a\)](#) (but see [Sec. 4.2](#)).

[Panel \(b\)](#) of [Fig. 2](#) illustrates that the regions with higher R_{PAH} have, in general, a higher ratio of $F_{1130W}/F_{770W} \propto F_{11.3\mu\text{m}}/F_{7.7\mu\text{m}}$. This ratio is often used as a diagnostic of the neutral-to-ionized PAH ratio (e.g. [Draine & Li 2001](#); [Maragkoudakis et al. 2018](#)). Neutral PAHs have a higher ratio of $F_{11.3\mu\text{m}}/F_{7.7\mu\text{m}}$, which decreases as the fraction of ionized PAHs increases. Thus, the distribution of F_{1130W}/F_{770W} shown in this plot is consistent with a scenario where the PAHs are ionized and destroyed in the H II regions with higher ionization parameter. Note, however, that this ratio can be affected by changes of the PAH size in higher intensity and harder radiation fields. The PAH feature at $3.3\mu\text{m}$, together with $F_{11.3\mu\text{m}}/F_{7.7\mu\text{m}}$, can help to disentangle the impact of PAH size from variations in the radiation field ([Draine et al. 2021](#); [Dale et al. 2022](#)). We refer the reader to [Chastenot et al. \(subm.b\)](#), who demonstrate that PAHs are not only more ionized, but also have smaller sizes in H II regions, which is consistent with their gradual destruction in such environments.

[Panel \(c\)](#) of [Fig. 2](#) provides some tentative conversions from the empirical correlations in [Panels \(a\) and \(b\)](#) towards a more physical interpretation. It shows $\log(R_{\text{PAH}})$ vs f_{ion} – the ionization fraction of hydrogen in each H II region. The latter is calculated from $\log([\text{S III}]/[\text{S II}])$ using the empirical parametrization from [Kreckel et al. \(2022\)](#). The color corresponds to the number of ionizing photons required to produce the observed $\text{H}\alpha$ luminosity $L(\text{H}\alpha)$: $Q^0 \simeq 7.33 \times 10^{11} L(\text{H}\alpha)$ assuming $T_e = 10000 \text{ K}$ ([Osterbrock & Ferland 2006](#)), and with $L(\text{H}\alpha)$ expressed in units of erg s^{-1} . In this representation, two different sequences are suggested when examining the dependence of PAH fraction on f_{ion} .

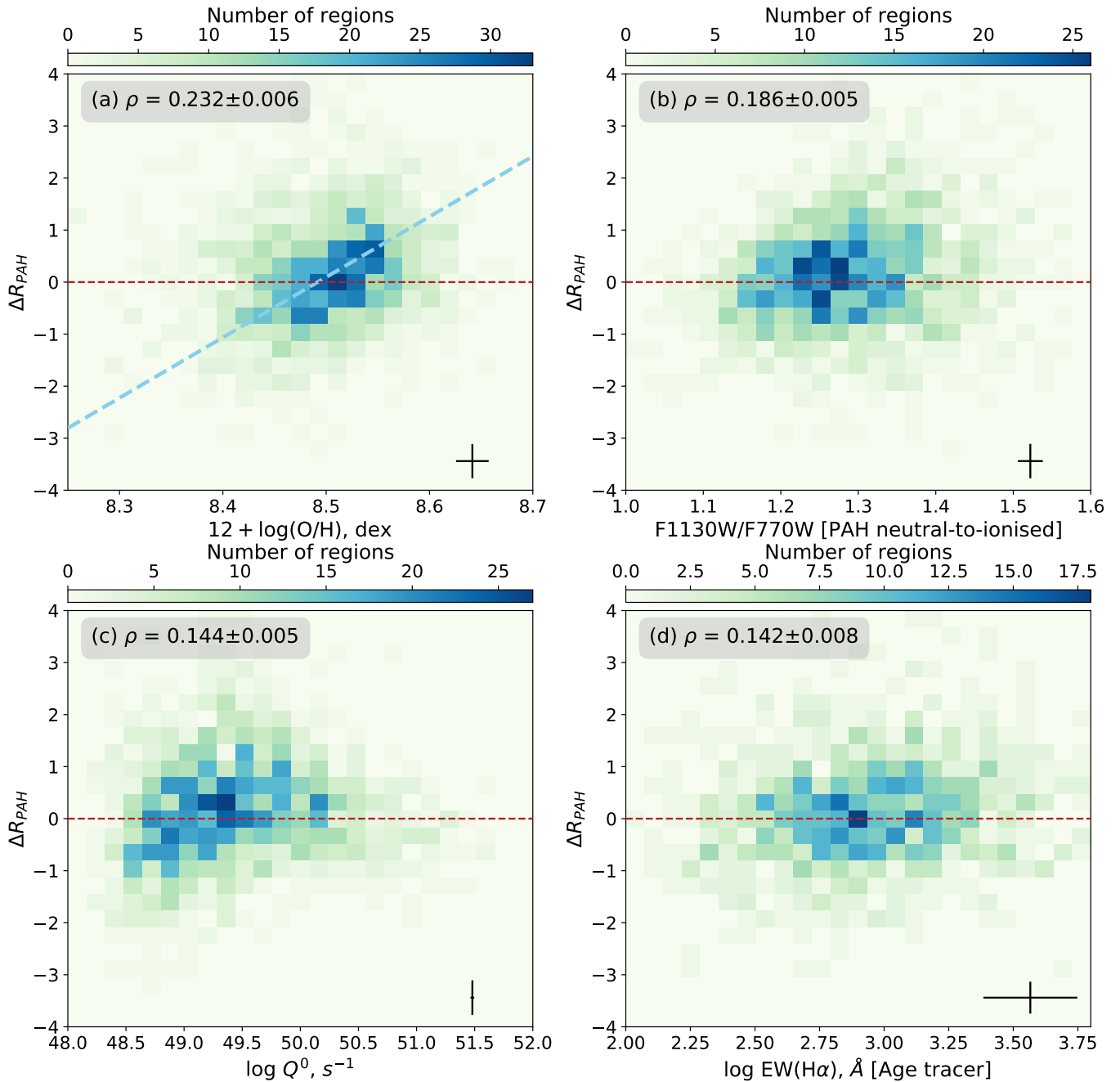


Figure 3. Secondary dependence of the PAH fraction on: the oxygen abundance of H II regions, measured as $12 + \log(\text{O}/\text{H})$ (Panel a); the F1130W/F770W flux ratio, sensitive to the relative fraction of neutral to ionized PAH (Panel b); the number of hydrogen ionizing photons Q^0 (Panel c); the equivalent width of $\text{H}\alpha$, corrected for the contribution of the underlying old stellar population (Panel d). The 2D histograms on each panel show the distribution of ΔR_{PAH} , obtained after subtracting of the values derived by Eq. 2 from the measured R_{PAH} . The red dashed line shows a zero-difference level. The light-blue dashed line on Panel (a) corresponds to a linear fit defined by Eq. 5, tracing the secondary relation of R_{PAH} on metallicity. The Spearman’s correlation coefficient (ρ) is given in the corner of each plot. Its uncertainty is derived in the same way as in Fig. 2. The error bars in the right-hand corner correspond to the 95th-percentile uncertainties of the measured values.

Namely, R_{PAH} only slightly decreases with increasing f_{ion} (and ionization parameter) for fainter H II regions, even when the ionization fraction is high. In turn, bright regions (likely associated with more massive star clusters) more strongly affect the PAH fraction. We perform separate linear fits to the faint and bright H II regions (shown by green and magenta dashed lines in Fig. 2c, respectively):

$$\log(R_{\text{PAH}})_{Q^0 < 10^{50}} = (-1.7 \pm 0.2)f_{\text{ion}} + (2.2 \pm 0.2), \quad (3)$$

$$\log(R_{\text{PAH}})_{Q^0 > 10^{50}} = (-14.2 \pm 1.4)f_{\text{ion}} + (14.2 \pm 1.3), \quad (4)$$

Given the well-known size – luminosity relation for H II regions (e.g. Wisnioski et al. 2012), a probable explanation of the bi-modality of the $\log(R_{\text{PAH}})$ vs f_{ion} relation is a difference in their sizes. This difference can have both a physical or observational origin (or a combination). On the one hand, the larger, brighter regions might encompass the full scale height of the galactic disk and exhibit $q_{\text{PAH}} \sim 0$ because the ISM is fully ionized towards these regions. On the other hand, the size of regions that are unresolved with MUSE might be overestimated, while for well-resolved regions the reprojected masks (see Section 3.1) should better isolate the H II regions. Thus, in the unresolved regions one may expect to see a higher contribution from the diffuse ISM to the measurements. The effects leading to the redistribution of the dust grains at the outskirts of H II regions (mentioned in Sec. 3.2) may also be more prominent. Panel (d) of Fig. 2 shows the same plot as Panel (c), but all points are color-coded by R/PSF – their effective angular radius relative to the resolution (FWHM of PSF) of the MUSE data. The color dashed lines show the regressions as on Panel (c) defined by Eqs. 3,4. Indeed, we start to resolve the H II regions with MUSE at $Q^0 \sim 10^{50} \text{ s}^{-1}$, which naturally explains the bi-modality. Future *JWST* observations of more nearby galaxies will help to clarify if the differences between the faint and bright H II regions are real, or just an effect of the limited resolution. Note that excluding the unresolved regions with $R/PSF < 1$ (64% of our sample) from consideration in Panels (a – c) of Fig. 2 does not affect our results, but the resolved regions do demonstrate a much tighter correlation with $\log([\text{S III}]/[\text{S II}])$ (see Appendix B).

In our measurements we do not attempt to correct for the contribution of the diffuse ISM to the optical emission line fluxes, or to the mid-IR bands, because performing a local background subtraction depends heavily on the exact H II region boundaries we define and potentially introduces large uncertainties into our measurements. Nevertheless, we validate in Appendix B that our results do not change if we keep only those regions where the background emission is negligible compared to our

measured fluxes. From this, we conclude that unresolved regions and contamination by the DIG/background mid-IR emission do not change our results, but are responsible for the scatter in Fig. 2.

4.2. Dependence of the PAH abundance on metallicity

The dependence of the PAH abundance on metallicity has been explored for galaxy-wide scales and for individual large star-forming complexes (e.g. Engelbracht et al. 2005; Khramtsova et al. 2013; Aniano et al. 2020). While q_{PAH} is clearly systematically lower in dwarf galaxies compared to spiral galaxies, in the high-metallicity regime this relation exhibits a considerable scatter. The galaxies in our sample have relatively high metallicity, and cover only 0.3 dex of dynamic range ($8.3 < 12 + \log(\text{O}/\text{H}) < 8.6$), which could contribute to the lack of a clear secondary dependence of R_{PAH} with oxygen abundance in Fig. 2a.

To explore the secondary dependence of R_{PAH} with metallicity, we subtract the relation in Eq. 2 from our measurements and correlate the residuals ΔR_{PAH} with $12 + \log(\text{O}/\text{H})$ in Fig. 3a. We find a mild correlation between these values only considering the 2D histogram representing the statistical density of the points on this plot. This correlation can be parameterized linearly as:

$$\Delta R_{\text{O}/\text{H}} = (11.3 \pm 0.5) \times ([12 + \log(\text{O}/\text{H})] - 8.69) + (2.2 \pm 0.1). \quad (5)$$

Using this $\Delta R_{\text{O}/\text{H}}$ in Eq. 2, we can describe the PAH fraction in H II regions as a function of characteristics of the ionized gas – its ionization parameter and metallicity. The dominant factor defining R_{PAH} is the ionization parameter, and the metallicity plays only a minor role leading to scatter in Fig. 2a,b. Note that we do not find any prominent secondary relation of the PAH fraction on other parameters (F1130W/F770W, Q^0) explored in Fig. 2 (the bend in the trend for Q^0 in Fig. 3c is probably due to the bi-modality discussed in Sec. 4.1).

To demonstrate that we are not missing a primary correlation between R_{PAH} and metallicity, we show the 2D histogram distribution of these values in Fig. 4a. Red symbols on this plot correspond to the values averaged over all regions within each galaxy. These averaged values show an expected mild trend of increasing PAH fraction with the higher metallicity. At the same time, the distribution of the individual H II regions demonstrates the opposite trend – a very weak anti-correlation of R_{PAH} with oxygen abundance (similarly to that for a small sample of high-metallicity galaxies in Engelbracht et al. 2008).

Overall, we conclude that the PAH destruction in H II regions is nearly independent of metallicity, at least for

the range of oxygen abundances we consider. Analyzing highly-resolved data for the LMC and SMC, [Chasten et al. \(2019\)](#) also found similar q_{PAH} in the luminous H II regions of those two galaxies, despite their difference in metallicity and a difference in their global q_{PAH} values. This supports our claim that the weakness of the metallicity dependence is not only due to the limited range of $12 + \log(\text{O}/\text{H})$ in our data. At the same time, [Chasten et al. \(subm.a\)](#) find a much stronger correlation between R_{PAH} and the metallicity of the diffuse ISM, where the intensity of H α is low. These results together imply that the metallicity regulates the PAH destruction and formation processes, but it becomes much less important in the H II regions, where the presence of large amount of ionized gas and intense ionizing radiation plays a dominant role.

4.3. The role of UV hardness

The PAH fraction in H II regions strongly correlates with the $[\text{S III}]/[\text{S II}]$ line ratio, with only a mild secondary dependence on the metallicity. While $[\text{S III}]/[\text{S II}]$ is a good tracer of the ionization parameter, it is also weakly dependent on the hardness of the UV radiation field (see Appendix A). Many previous studies found a correlation between the PAH fraction and the hardness of the radiation field at the scale of star-forming complexes (e.g. [Madden et al. 2006](#); [Gordon et al. 2008](#); [Khramtsova et al. 2014](#); [Maragkoudakis et al. 2018](#)), and thus we cannot be sure that the trend seen in Fig. 2 is driven by the intensity of the hydrogen-ionizing radiation (or ionization parameter) and not by the hardness of the ionizing radiation field.

We cannot directly measure the hardness of the UV field from our data, but as was shown by [Levesque et al. \(2010\)](#) and [Khramtsova et al. \(2014\)](#) (see also Fig. 5 in Appendix A), $[\text{O III}]/\text{H}\beta$ is a reasonable tracer of UV hardness at fixed metallicity. This ratio also depends on the ionization parameter, but to a lesser extent than $[\text{S III}]/[\text{S II}]$. Given this, we would expect to see a strong correlation between R_{PAH} and $[\text{O III}]/\text{H}\beta$ if the PAH destruction in H II regions is regulated mostly by the hardness of the ionizing radiation field, and not by its intensity. In fact, we see only a relatively weak correlation between these parameters in Fig. 4c. Note that our result remains unchanged if we exclude IC 5332 from consideration (and only focus on the three galaxies of approximately similar metallicity). Thus, it is probable that it is indeed the ionization parameter, and not hardness, that drives the correlation in Fig. 2.

4.4. Towards an evolutionary sequence

The dependence of R_{PAH} on the ionization parameter can be viewed within the context of an H II region evolu-

tionary sequence. We expect the ionization parameter to decrease with age, as older star clusters produce fewer ionizing photons and the H II region expands ([Dopita et al. 2006](#)). The equivalent width of Balmer lines (e.g., $EW(\text{H}\alpha)$) is another (more common) indicator that decreases with the age of an H II region ([Levesque & Leitherer 2013](#)). In Fig. 4b, we identify a correlation between R_{PAH} and $EW(\text{H}\alpha)$, where $EW(\text{H}\alpha)$ has been corrected for the contribution of the underlying old stellar population⁵. R_{PAH} decreases with $EW(\text{H}\alpha)$, however the correlation is not as prominent as the correlation with $[\text{S III}]/[\text{S II}]$. This suggests that the fraction of PAH molecules in the total dust mass increases slightly with time, if we assume that $EW(\text{H}\alpha)$ is a good tracer of the age of H II region. Note that we do not find a secondary correlation between the residuals ΔR_{PAH} (obtained after subtraction of the relation defined by Eq. 2 from the observed data) on $EW(\text{H}\alpha)$ (Fig. 3d), probably because both $EW(\text{H}\alpha)$ and $[\text{S III}]/[\text{S II}]$ should decrease with the age. If such correlation with age is real, then it implies that the PAH fraction is higher in older regions. This can be explained if we assume that the balance between PAH formation and destruction changes with time. For example, the relative fraction of PAHs can increase with time if the very small grains have been destroyed or cleared from the older H II regions more efficiently than PAHs, or if PAHs (even gradually) build up as result of destruction of larger dust grains (e.g., as results of shattering).

Previous studies have revealed a possible evolution of the PAH abundance with the age of star-forming regions, but the behavior is quite complex and depends on the balance between the processes of formation and destruction of the dust grains and PAHs (e.g. [Wiebe et al. 2014](#); [Khramtsova et al. 2014](#); [Lin et al. 2020](#)). In particular, according to [Khramtsova et al. \(2014\)](#), R_{PAH} increases with age for low-metallicity regions, and this trend flattens for higher metallicities. The correlation of R_{PAH} with $EW(\text{H}\alpha)$ in Fig. 4b is relatively weak, and $EW(\text{H}\alpha)$ itself is not always a strong tracer of H II region age ([Scheuermann et al., in prep.](#)), thus we are hesitant to interpret this trend as strong evidence for an age sequence. Future work linking H II regions with age dating of ionizing stellar clusters using PHANGS-HST and PHANGS-JWST data will provide a more robust quantification of these tentative age trends (see also [Dale et al. 2022](#)).

⁵ This correction is performed by subtracting the corresponding continuum derived in a circular aperture surrounding each H II region. For details, see [Scheuermann et al. \(submitted\)](#)

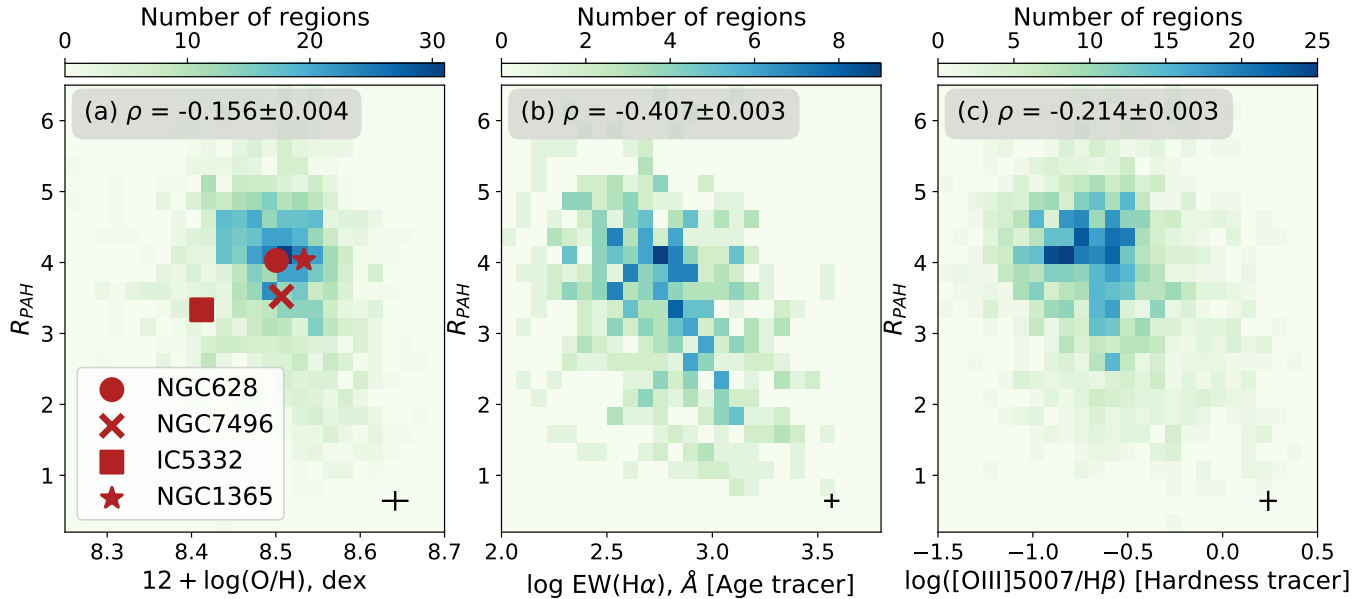


Figure 4. Correlation of the PAH fraction, traced by R_{PAH} , with different physical conditions. Panel a: correlation with oxygen abundance, $12 + \log(\text{O}/\text{H})$, with red symbols showing the mean value for each galaxy. Panel b: equivalent width of $\text{H}\alpha$, $\text{EW}(\text{H}\alpha)$, corrected for the contribution of the underlying old stellar population, and a tracer of H II region age. Note that because of the large uncertainty introduced by this background continuum subtraction, we consider here only regions with relative error $\delta(\text{EW}(\text{H}\alpha)) < 10\%$. Panel c: $\log([\text{O III}]/\text{H}\beta)$, a tracer of the hardness of the UV radiation. The Spearman’s correlation coefficient (ρ) is given in the corner of each plot. Its uncertainty is derived in the same way as in Fig. 2. The error bars in the right-hand corner correspond to the 95th-percentile uncertainties of the measured values.

4.5. The role of shocks

Beyond the correlations identified in this letter, we search for other properties regulating the PAH fraction on the scales of individual H II regions. In particular, we tested whether shocks affect the PAH fraction by considering regions associated with high $\text{H}\alpha$ velocity dispersion (Egorov et al., in prep.) or classified as shock ionized by diagnostic optical emission lines ratios (Congiu et al., submitted), but did not find any significant differences from the trends we identify using the H II regions in Fig. 2. Thus, the ionization parameter (intensity of hydrogen-ionizing radiation) appears to be the dominant factor in defining the mechanisms for PAH destruction in H II regions.

5. SUMMARY

With *JWST* it is now possible to systematically study the properties of the PAH component of the ISM at the scales of individual H II regions in the galaxies beyond our Local Group, building a more representative picture of the interplay between ionizing sources and dust properties. As a pilot study, we analyze the PAH fraction in 1529 H II regions within the disks of four nearby star-forming galaxies from the PHANGS-*JWST* program, and compare them with the properties of the ionized gas as obtained from PHANGS-MUSE observations. We find a strong anti-correlation between PAH

fraction and ionization parameter, with a steeper dependence for more luminous regions. This is consistent with a scenario where the destruction of the PAH molecules is set by the hydrogen-ionizing UV radiation, though it is not clear if the observed trend reflects an evolutionary sequence. We find only a weak secondary dependence between PAH fraction and oxygen abundance, although we note that we cover a very limited range (~ 0.3 dex) in metallicity in our sample. Together with the results presented in Chastenot et al. (subm.a), this implies that, in contrast to the diffuse ISM, the metallicity becomes unimportant in defining the balance between PAHs formation and destruction in H II regions, where the presence of ionized gas and hard radiation dominate.

In this study leveraging new *JWST* observations for four star-forming galaxies, we have demonstrated that hydrogen-ionizing UV radiation is the dominant mechanism for PAH destruction in H II regions.

ACKNOWLEDGMENTS

This work is based on observations made with the NASA/ESA/CSA *JWST*. The data were obtained from the Mikulski Archive for Space Telescopes at the Space Telescope Science Institute, which is operated by the Association of Universities for Research in Astronomy, Inc., under NASA contract NAS 5-03127. The observations are associated with *JWST* program 2107.

The specific observations analyzed can be accessed via [10.17909/9bdf-jn24](https://doi.org/10.17909/9bdf-jn24). Based on observations collected at the European Southern Observatory under ESO programmes 094.C-0623 (PI: Kreckel), 095.C-0473, 098.C-0484 (PI: Blanc), 1100.B-0651 (PHANGS-MUSE; PI: Schinnerer), as well as 094.B-0321 (MAGNUM; PI: Marconi), 099.B-0242, 0100.B-0116, 098.B-0551 (MAD; PI: Carollo) and 097.B-0640 (TIMER; PI: Gadotti).

KK, OE and FS gratefully acknowledge funding from the Deutsche Forschungsgemeinschaft (DFG, German Research Foundation) in the form of an Emmy Noether Research Group (grant number KR4598/2-1, PI Kreckel). EJW, RSK, SCOG acknowledge funding from the Deutsche Forschungsgemeinschaft (DFG, German Research Foundation) – Project-ID 138713538 – SFB 881 (“The Milky Way System”, subprojects A1, B1, B2, B8, P1). HAP acknowledges support by the National Science and Technology Council of Taiwan under grant 110-2112-M-032-020-MY3. TGW and ES acknowledge funding from the European Research Council (ERC) under the European Union’s Horizon 2020 research and innovation programme (grant agreement No. 694343). MB acknowledges support from FONDECYT regular grant 1211000 and by the ANID BASAL project FB210003. JMDK gratefully acknowledges funding from the European Research Council (ERC) under the European Union’s Horizon 2020 research and innovation programme via the ERC Starting Grant MUSTANG (grant agreement number 714907). COOL Research DAO is a Decentralized Autonomous Organization supporting research in astrophysics aimed at uncovering our cosmic origins. E.C. acknowledges support from ANID Basal projects ACE210002 and FB210003. FB would like to acknowledge funding from the European Research Council (ERC) under the European Union’s Horizon 2020 research and innovation programme (grant agreement No.726384/Empire)

MC gratefully acknowledges funding from the DFG through an Emmy Noether Research Group (grant number CH2137/1-1). RSK and SCOG acknowledge support from the European Research Council via the ERC Synergy Grant “ECOGAL” (project ID 855130), from the Heidelberg Cluster of Excellence (EXC 2181 - 390900948) “STRUCTURES”, funded by the German Excellence Strategy, and from the German Ministry for Economic Affairs and Climate Action for funding in project “MAINN” (funding ID 500O2206). ER acknowledges the support of the Natural Sciences and Engineering Research Council of Canada (NSERC), funding reference number RGPIN-2022-03499. KG is supported by the Australian Research Council through the Discovery Early Career Researcher Award (DECRA) Fellowship DE220100766 funded by the Australian Government. KG is supported by the Australian Research Council Centre of Excellence for All Sky Astrophysics in 3 Dimensions (ASTRO 3D), through project number CE170100013. G.A.B. acknowledges the support from ANID Basal project FB210003. JC acknowledges support from ERC starting grant #851622 DustOrigin. AKL gratefully acknowledges support by grants 1653300 and 2205628 from the National Science Foundation, by award JWST-GO-02107.009-A, and by a Humboldt Research Award from the Alexander von Humboldt Foundation. JPe acknowledges support by the DAOISM grant ANR-21-CE31-0010 and by the Programme National “Physique et Chimie du Milieu Interstellaire” (PCMI) of CNRS/INSU with INC/INP, co-funded by CEA and CNES.

Facilities: JWST(MIRI), VLT(MUSE)

Software: Astropy (Astropy Collaboration et al. 2013, 2018), Cloudy (Ferland et al. 2017), pyCloudy (Morisset 2013), Starburst99 (Leitherer et al. 1999, 2014), WebbPSF (Perrin et al. 2014)

APPENDIX

A. PHYSICAL INTERPRETATION OF EMISSION LINE RATIOS IN THE CONTEXT OF PHOTOIONIZATION MODELING

Here we consider how the hardness and intensity of the ionizing radiation impact the $[S\text{ III}]/[S\text{ II}]$ and $[O\text{ III}]/H\beta$ line ratios, and how they evolve with the age of the H II regions. Kreckel et al. (2022) presented STARBURST99 (Leitherer et al. 1999, 2014) and CLOUDY (Ferland et al. 2017) models computed for a grid of star clusters and H II region physical properties matched to the observed properties as derived in the PHANGS-MUSE and PHANGS-HST data. Here we use a sub-set of their models for metallicity $Z \sim 0.6Z_{\odot}$ (approximately equal to the metallicity of the four galaxies considered in this work, see Table 1). We consider clusters of mass $\log(M_*/M_{\odot}) = 3.5, 4.5, 5.5$ and age $t = 1...9$ Myr (with step of 1 Myr) as the ionizing source of a cloud with constant hydrogen density $n_{\text{H}} \simeq n_{\text{e}} = 20, 90, 300\text{ cm}^{-3}$. For simplicity, here we consider only one nebular geometry – a shell with an inner radius of 15 pc, and filling factor $ff = 1$.

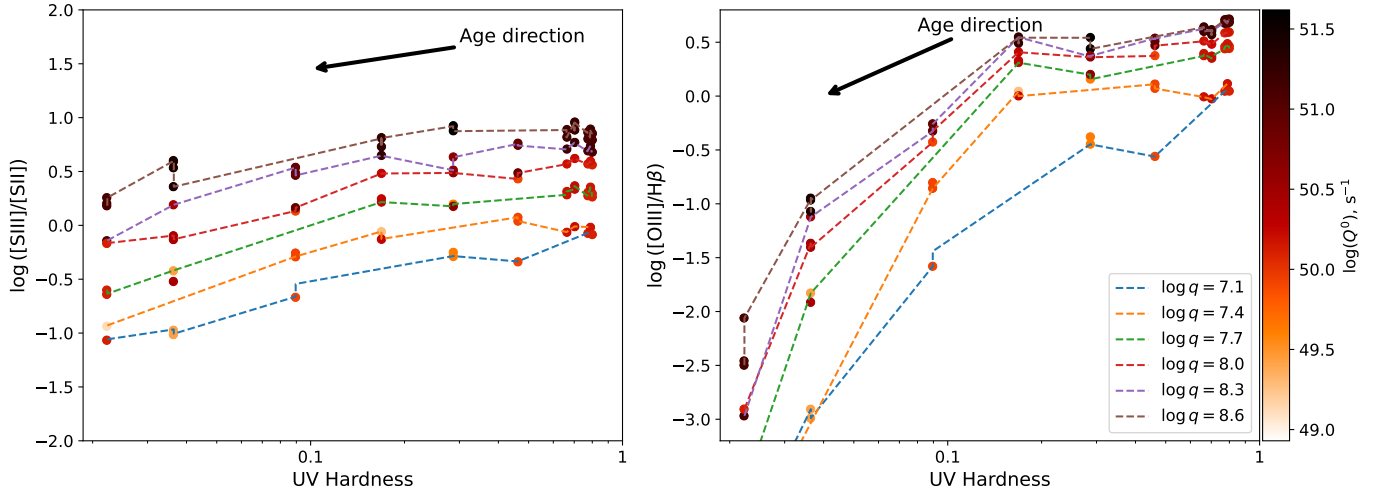


Figure 5. Dependence of $[S\ III]/[S\ II]$ (left-hand panel) and $[O\ III]/H\beta$ (right-hand panel) optical emission line ratios on the hardness of the ionizing UV radiation and on the ionization parameter q , according to a grid of STARBURST99 and CLOUDY models (see text). Different points are the individual nodes of the model grid, defined by the different mass and age of the ionizing cluster and the density of the $H\ II$ region. The color of the points encodes the number of hydrogen-ionizing photons, Q^0 .

Similar to [Khramtsova et al. \(2014\)](#), we parameterize the hardness of the UV radiation as the ratio of the total flux in the ionizing continuum at short wavelengths (20 Å to 912 Å) to that at longer wavelengths (912 Å to 2000 Å). Fig. 5 shows how both ionization parameter and UV hardness are traced by the emission line ratios $[S\ III]/[S\ II]$ and $[O\ III]/H\beta$. These line ratios are sensitive to both parameters, but $[S\ III]/[S\ II]$ shows a stronger dependence on the ionization parameter, while $[O\ III]/H\beta$ is less sensitive to ionization parameter but varies significantly with the hardness of the UV radiation. Thus, by analyzing the dependence of PAH fraction in $H\ II$ regions using both of these line ratios, we can disentangle whether UV hardness or the number of ionizing photons (proportional to the ionization parameter) is the main driver for PAH destruction. We consider this in Sec. 4.3.

B. TESTING THE IMPACT OF LIMITED ANGULAR RESOLUTION AND CONTAMINATION BY EMISSION FROM THE DIFFUSE ISM

As we show in Section 4.1, a large fraction of the $H\ II$ regions analyzed in this paper are not well-resolved by our PHANGS-MUSE observations ($R/PSF < 1$ in Fig. 2d). Also, we do not correct the measured fluxes of the optical emission lines and mid-IR bands for a local background, as implementing such subtraction is a fairly uncertain process. Nevertheless, both these factors may affect our measurements. In order to check that our conclusions are not biased because of these factors, we perform several tests in this Section.

In unresolved $H\ II$ regions, the measured value of R_{PAH} may be biased because of a larger contribution from the surrounding PDR and diffuse ISM to the aperture, which is indeed seen in Fig. 2d. In Fig. 6 we repeat the analysis presented in Sec. 4.1, but consider only the resolved $H\ II$ regions having $R/PSF > 1$ (44% of total number of $H\ II$ regions in the analysis). As shown, the relations drawn from the entire sample are the same (but tighter) as the relations observed for the resolved $H\ II$ regions alone.

The second test shown in Fig. 6 allows us to confirm that the contamination by the diffuse ISM does not introduce a bias to our results. Here we follow the same approach as in [Kreckel et al. \(2022\)](#) – we consider only the $H\ II$ regions with a significant contrast in the $H\alpha$ and $[S\ II]$ fluxes and in the mid-IR bands compared to the local background. We estimate the contrast as the maximal value of $C = F_{HII}/(I_{bgr} \times S)$ among all considered lines/bands, where F_{HII} is a measured integral flux of the $H\ II$ region, I_{bgr} is the median brightness of the surrounding local background estimated across a $10''$ circular aperture after masking all $H\ II$ regions, and S is the area within the $H\ II$ region mask. In Fig. 6 we show only regions with a contrast $C > 2$, for which the contribution of the diffuse emission to the total flux is negligible ($\sim 29\%$ of the entire sample). This ‘clear’ sample demonstrates the same trends as the entire sample in Fig. 2.

We may thus conclude that the presence of unresolved $H\ II$ regions and contamination by the diffuse ISM (which is still unavoidable for galaxies outside the Local Group) does not affect the results of our analysis, but add scatter to the observed relations. Note, however, that when considering these sub-samples we cannot judge how reliable our findings

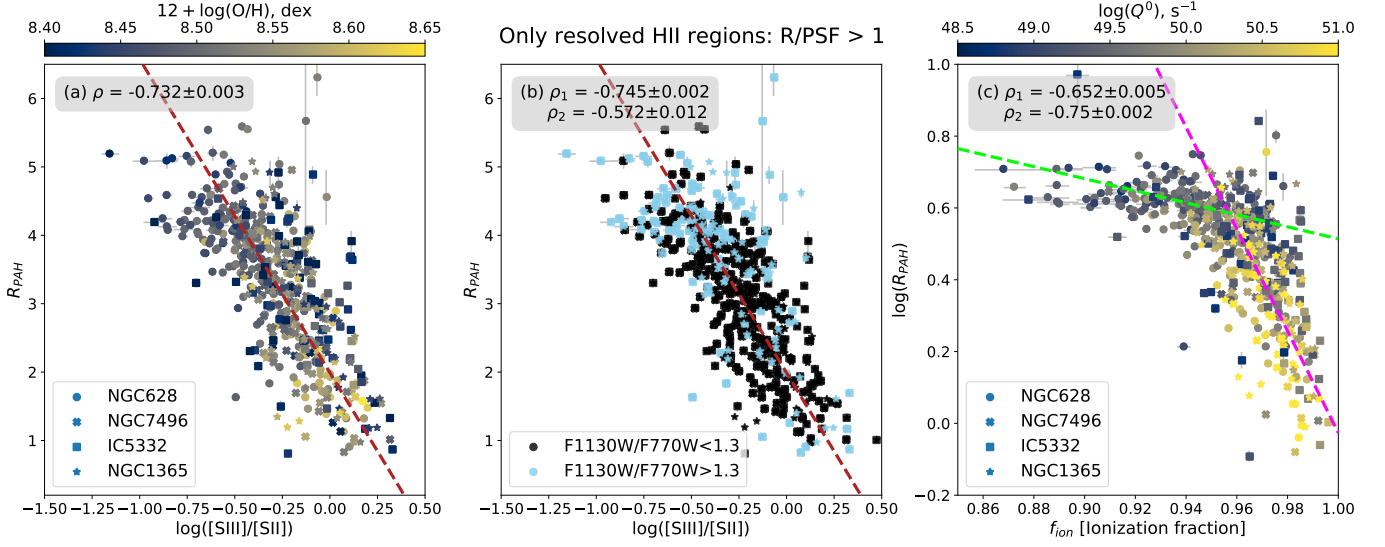


Figure 6. Same as in Fig. 2(a–c), but for the resolved H II regions only (those with $R/PSF > 1$ in Fig. 2d). The colored lines show the same linear regressions as in Fig. 2.

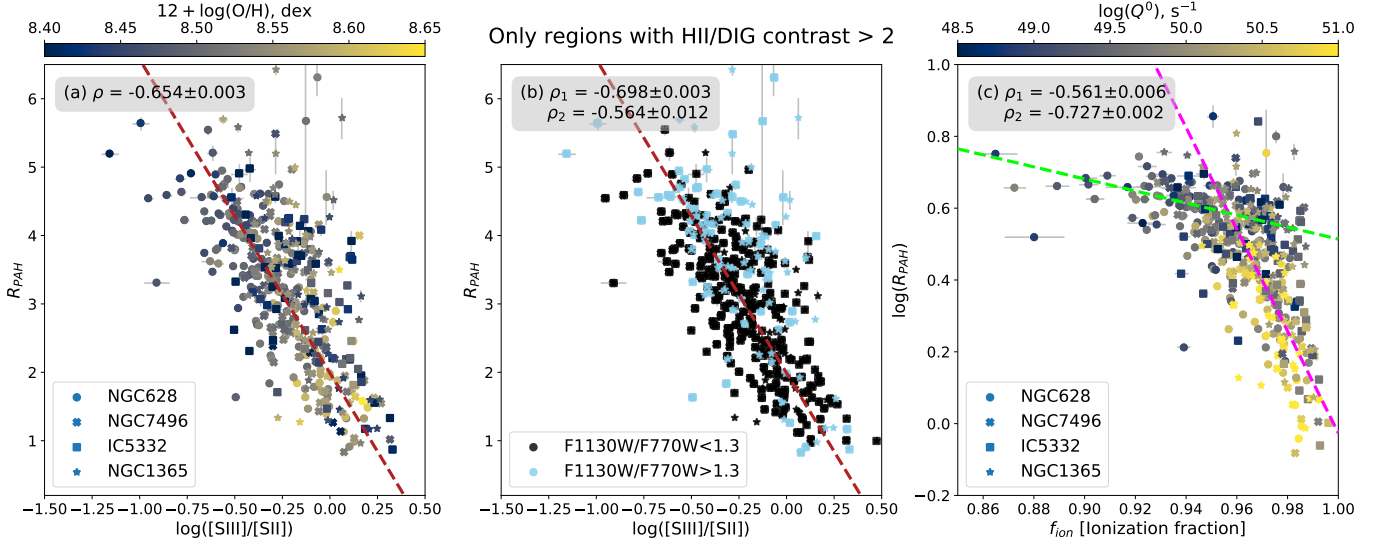


Figure 7. Same as in Fig. 6, but for a sub-sample of the H II regions with a large contrast against the surrounding local background in the $H\alpha$, $[S II]$ emission lines and mid-IR bands.

are regarding the secondary dependence of the PAH fraction on metallicity (Sec. 4.2, Fig. 3) because the number of regions at the low-metallicity end of the ‘clear’ samples analyzed is too small.

REFERENCES

- Allain, T., Leach, S., & Sedlmayr, E. 1996, *A&A*, 305, 602
- Anand, G. S., Lee, J. C., Van Dyk, S. D., et al. 2021a, *MNRAS*, 501, 3621, doi: [10.1093/mnras/staa3668](https://doi.org/10.1093/mnras/staa3668)
- Anand, G. S., Rizzi, L., Tully, R. B., et al. 2021b, *AJ*, 162, 80, doi: [10.3847/1538-3881/ac0440](https://doi.org/10.3847/1538-3881/ac0440)
- Anderson, L. D., Bania, T. M., Bialer, D. S., et al. 2014, *ApJS*, 212, 1, doi: [10.1088/0067-0049/212/1/1](https://doi.org/10.1088/0067-0049/212/1/1)
- Aniano, G., Draine, B. T., Gordon, K. D., & Sandstrom, K. 2011, *PASP*, 123, 1218, doi: [10.1086/662219](https://doi.org/10.1086/662219)
- Aniano, G., Draine, B. T., Hunt, L. K., et al. 2020, *ApJ*, 889, 150, doi: [10.3847/1538-4357/ab5fdb](https://doi.org/10.3847/1538-4357/ab5fdb)

- Astropy Collaboration, Robitaille, T. P., Tollerud, E. J., et al. 2013, *A&A*, 558, A33, doi: [10.1051/0004-6361/201322068](https://doi.org/10.1051/0004-6361/201322068)
- Astropy Collaboration, Price-Whelan, A. M., Sipőcz, B. M., et al. 2018, *AJ*, 156, 123, doi: [10.3847/1538-3881/aabc4f](https://doi.org/10.3847/1538-3881/aabc4f)
- Bacon, R., Accardo, M., Adjali, L., et al. 2010, in *Society of Photo-Optical Instrumentation Engineers (SPIE) Conference Series*, Vol. 7735, *Ground-based and Airborne Instrumentation for Astronomy III*, ed. I. S. McLean, S. K. Ramsay, & H. Takami, 773508, doi: [10.1117/12.856027](https://doi.org/10.1117/12.856027)
- Baldwin, J. A., Phillips, M. M., & Terlevich, R. 1981, *PASP*, 93, 5, doi: [10.1086/130766](https://doi.org/10.1086/130766)
- Belfiore, F., Santoro, F., Groves, B., et al. 2022, *A&A*, 659, A26, doi: [10.1051/0004-6361/202141859](https://doi.org/10.1051/0004-6361/202141859)
- Binder, B. A., & Povich, M. S. 2018, *ApJ*, 864, 136, doi: [10.3847/1538-4357/aad7b2](https://doi.org/10.3847/1538-4357/aad7b2)
- Bocchio, M., Micelotta, E. R., Gautier, A. L., & Jones, A. P. 2012, *A&A*, 545, A124, doi: [10.1051/0004-6361/201219705](https://doi.org/10.1051/0004-6361/201219705)
- Bolatto, A. D., Simon, J. D., Stanimirović, S., et al. 2007, *ApJ*, 655, 212, doi: [10.1086/509104](https://doi.org/10.1086/509104)
- Burkhardt, A. M., Long Kelvin Lee, K., Bryan Changala, P., et al. 2021, *ApJL*, 913, L18, doi: [10.3847/2041-8213/abfd3a](https://doi.org/10.3847/2041-8213/abfd3a)
- Calzetti, D. 2013, in *Secular Evolution of Galaxies*, ed. J. Falcón-Barroso & J. H. Knapen (Cambridge University Press), 419
- Chastenet, J., Bot, C., Gordon, K. D., et al. 2017, *A&A*, 601, A55, doi: [10.1051/0004-6361/201629133](https://doi.org/10.1051/0004-6361/201629133)
- Chastenet, J., Sandstrom, K., Chiang, I.-D., et al. 2019, *ApJ*, 876, 62, doi: [10.3847/1538-4357/ab16cf](https://doi.org/10.3847/1538-4357/ab16cf)
- Chastenet, J., et al. subm.a, *ApJL*
- . subm.b, *ApJL*
- Cherchneff, I., Barker, J. R., & Tielens, A. G. G. M. 1992, *ApJ*, 401, 269, doi: [10.1086/172059](https://doi.org/10.1086/172059)
- Dale, D. A., Boquien, M., Barnes, A. T., et al. 2022, *arXiv e-prints*, arXiv:2212.00130, <https://arxiv.org/abs/2212.00130>
- Dopita, M. A., Fischera, J., Sutherland, R. S., et al. 2006, *ApJ*, 647, 244, doi: [10.1086/505418](https://doi.org/10.1086/505418)
- Draine, B. T. 2011, *ApJ*, 732, 100, doi: [10.1088/0004-637X/732/2/100](https://doi.org/10.1088/0004-637X/732/2/100)
- Draine, B. T., & Li, A. 2001, *ApJ*, 551, 807, doi: [10.1086/320227](https://doi.org/10.1086/320227)
- . 2007, *ApJ*, 657, 810, doi: [10.1086/511055](https://doi.org/10.1086/511055)
- Draine, B. T., Li, A., Hensley, B. S., et al. 2021, *ApJ*, 917, 3, doi: [10.3847/1538-4357/abff51](https://doi.org/10.3847/1538-4357/abff51)
- Emsellem, E., Schinnerer, E., Santoro, F., et al. 2022, *A&A*, 659, A191, doi: [10.1051/0004-6361/202141727](https://doi.org/10.1051/0004-6361/202141727)
- Engelbracht, C. W., Gordon, K. D., Rieke, G. H., et al. 2005, *ApJL*, 628, L29, doi: [10.1086/432613](https://doi.org/10.1086/432613)
- Engelbracht, C. W., Rieke, G. H., Gordon, K. D., et al. 2008, *ApJ*, 678, 804, doi: [10.1086/529513](https://doi.org/10.1086/529513)
- Everett, J. E., & Churchwell, E. 2010, *ApJ*, 713, 592, doi: [10.1088/0004-637X/713/1/592](https://doi.org/10.1088/0004-637X/713/1/592)
- Ferland, G. J., Chatzikos, M., Guzmán, F., et al. 2017, *RMxAA*, 53, 385. <https://arxiv.org/abs/1705.10877>
- Gail, H. P., & Sedlmayr, E. 1979, *A&A*, 77, 165
- García-Bernete, I., Rigopoulou, D., Alonso-Herrero, A., et al. 2022, *MNRAS*, 509, 4256, doi: [10.1093/mnras/stab3127](https://doi.org/10.1093/mnras/stab3127)
- Gordon, K. D., Engelbracht, C. W., Rieke, G. H., et al. 2008, *ApJ*, 682, 336, doi: [10.1086/589567](https://doi.org/10.1086/589567)
- Groves, B., Dopita, M. A., Sutherland, R. S., et al. 2008, *ApJS*, 176, 438, doi: [10.1086/528711](https://doi.org/10.1086/528711)
- Hirashita, H., & Yan, H. 2009, *MNRAS*, 394, 1061, doi: [10.1111/j.1365-2966.2009.14405.x](https://doi.org/10.1111/j.1365-2966.2009.14405.x)
- Hunt, L. K., Thuan, T. X., Izotov, Y. I., & Sauvage, M. 2010, *ApJ*, 712, 164, doi: [10.1088/0004-637X/712/1/164](https://doi.org/10.1088/0004-637X/712/1/164)
- Jensen, J. J., Hönig, S. F., Rakshit, S., et al. 2017, *MNRAS*, 470, 3071, doi: [10.1093/mnras/stx1447](https://doi.org/10.1093/mnras/stx1447)
- Jones, A. P., Tielens, A. G. G. M., & Hollenbach, D. J. 1996, *ApJ*, 469, 740, doi: [10.1086/177823](https://doi.org/10.1086/177823)
- Kewley, L. J., & Dopita, M. A. 2002, *ApJS*, 142, 35, doi: [10.1086/341326](https://doi.org/10.1086/341326)
- Kewley, L. J., Nicholls, D. C., & Sutherland, R. S. 2019, *ARA&A*, 57, 511, doi: [10.1146/annurev-astro-081817-051832](https://doi.org/10.1146/annurev-astro-081817-051832)
- Khramtsova, M. S., Wiebe, D. S., Boley, P. A., & Pavlyuchenkov, Y. N. 2013, *MNRAS*, 431, 2006, doi: [10.1093/mnras/stt319](https://doi.org/10.1093/mnras/stt319)
- Khramtsova, M. S., Wiebe, D. S., Lozinskaya, T. A., & Egorov, O. V. 2014, *MNRAS*, 444, 757, doi: [10.1093/mnras/stu1482](https://doi.org/10.1093/mnras/stu1482)
- Kourkchi, E., Courtois, H. M., Graziani, R., et al. 2020, *AJ*, 159, 67, doi: [10.3847/1538-3881/ab620e](https://doi.org/10.3847/1538-3881/ab620e)
- Kreckel, K., Egorov, O. V., Belfiore, F., et al. 2022, *A&A*, 667, A16, doi: [10.1051/0004-6361/202243858](https://doi.org/10.1051/0004-6361/202243858)
- Kumari, N., Amorín, R., Pérez-Montero, E., Vílchez, J., & Maiolino, R. 2021, *MNRAS*, 508, 1084, doi: [10.1093/mnras/stab2495](https://doi.org/10.1093/mnras/stab2495)
- Lai, T. S. Y., Armus, L., U, V., et al. 2022, *arXiv e-prints*, arXiv:2209.06741. <https://arxiv.org/abs/2209.06741>
- Latter, W. B. 1991, *ApJ*, 377, 187, doi: [10.1086/170346](https://doi.org/10.1086/170346)
- Lebouteiller, V., Bernard-Salas, J., Whelan, D. G., et al. 2011, *ApJ*, 728, 45, doi: [10.1088/0004-637X/728/1/45](https://doi.org/10.1088/0004-637X/728/1/45)
- Lee, J. C., Sandstrom, K. M., Leroy, A. K., et al. 2022a, *arXiv e-prints*, arXiv:2212.02667, <https://arxiv.org/abs/2212.02667>

- Lee, J. C., Whitmore, B. C., Thilker, D. A., et al. 2022b, *ApJS*, 258, 10, doi: [10.3847/1538-4365/ac1fe5](https://doi.org/10.3847/1538-4365/ac1fe5)
- Leitherer, C., Ekström, S., Meynet, G., et al. 2014, *ApJS*, 212, 14, doi: [10.1088/0067-0049/212/1/14](https://doi.org/10.1088/0067-0049/212/1/14)
- Leitherer, C., Schaerer, D., Goldader, J. D., et al. 1999, *ApJS*, 123, 3, doi: [10.1086/313233](https://doi.org/10.1086/313233)
- Leroy, A. K., Schinnerer, E., Hughes, A., et al. 2021, *ApJS*, 257, 43, doi: [10.3847/1538-4365/ac17f3](https://doi.org/10.3847/1538-4365/ac17f3)
- Levesque, E. M., Kewley, L. J., & Larson, K. L. 2010, *AJ*, 139, 712, doi: [10.1088/0004-6256/139/2/712](https://doi.org/10.1088/0004-6256/139/2/712)
- Levesque, E. M., & Leitherer, C. 2013, *ApJ*, 779, 170, doi: [10.1088/0004-637X/779/2/170](https://doi.org/10.1088/0004-637X/779/2/170)
- Li, A. 2020, *Nature Astronomy*, 4, 339, doi: [10.1038/s41550-020-1051-1](https://doi.org/10.1038/s41550-020-1051-1)
- Lin, Z., Calzetti, D., Kong, X., et al. 2020, *ApJ*, 896, 16, doi: [10.3847/1538-4357/ab9106](https://doi.org/10.3847/1538-4357/ab9106)
- Madden, S. C., Galliano, F., Jones, A. P., & Sauvage, M. 2006, *A&A*, 446, 877, doi: [10.1051/0004-6361:20053890](https://doi.org/10.1051/0004-6361:20053890)
- Mallory, K., Calzetti, D., & Lin, Z. 2022, *ApJ*, 933, 156, doi: [10.3847/1538-4357/ac7227](https://doi.org/10.3847/1538-4357/ac7227)
- Maragkoudakis, A., Ivkovich, N., Peeters, E., et al. 2018, *MNRAS*, 481, 5370, doi: [10.1093/mnras/sty2658](https://doi.org/10.1093/mnras/sty2658)
- Matsuura, M., Woods, P. M., & Owen, P. J. 2013, *MNRAS*, 429, 2527, doi: [10.1093/mnras/sts521](https://doi.org/10.1093/mnras/sts521)
- Matsuura, M., Barlow, M. J., Zijlstra, A. A., et al. 2009, *MNRAS*, 396, 918, doi: [10.1111/j.1365-2966.2009.14743.x](https://doi.org/10.1111/j.1365-2966.2009.14743.x)
- Micelotta, E. R., Jones, A. P., & Tielens, A. G. G. M. 2010a, *A&A*, 510, A36, doi: [10.1051/0004-6361/200911682](https://doi.org/10.1051/0004-6361/200911682)
- . 2010b, *A&A*, 510, A37, doi: [10.1051/0004-6361/200911683](https://doi.org/10.1051/0004-6361/200911683)
- Montillaud, J., Joblin, C., & Toubanc, D. 2013, *A&A*, 552, A15, doi: [10.1051/0004-6361/201220757](https://doi.org/10.1051/0004-6361/201220757)
- Morisset, C. 2013, *pyCloudy: Tools to manage astronomical Cloudy photoionization code*. <http://ascl.net/1304.020>
- Oey, M. S., López-Hernández, J., Kellar, J. A., et al. 2017, *ApJ*, 844, 63, doi: [10.3847/1538-4357/aa73d3](https://doi.org/10.3847/1538-4357/aa73d3)
- O'Halloran, B., Satyapal, S., & Dudik, R. P. 2006, *ApJ*, 641, 795, doi: [10.1086/500529](https://doi.org/10.1086/500529)
- Osterbrock, D. E., & Ferland, G. J. 2006, *Astrophysics of gaseous nebulae and active galactic nuclei*, 2nd edn. (University Science Books)
- Paladini, R., Umana, G., Veneziani, M., et al. 2012, *ApJ*, 760, 149, doi: [10.1088/0004-637X/760/2/149](https://doi.org/10.1088/0004-637X/760/2/149)
- Paturel, G., Petit, C., Prugniel, P., et al. 2003, *A&A*, 412, 45, doi: [10.1051/0004-6361:20031411](https://doi.org/10.1051/0004-6361:20031411)
- Pavlyuchenkov, Y. N., Kirsanova, M. S., & Wiebe, D. S. 2013, *Astronomy Reports*, 57, 573, doi: [10.1134/S1063772913070056](https://doi.org/10.1134/S1063772913070056)
- Perrin, M. D., Sivaramakrishnan, A., Lajoie, C.-P., et al. 2014, in *Society of Photo-Optical Instrumentation Engineers (SPIE) Conference Series*, Vol. 9143, *Space Telescopes and Instrumentation 2014: Optical, Infrared, and Millimeter Wave*, ed. J. Oschmann, Jacobus M., M. Clampin, G. G. Fazio, & H. A. MacEwen, 91433X, doi: [10.1117/12.2056689](https://doi.org/10.1117/12.2056689)
- Pilyugin, L. S., & Grebel, E. K. 2016, *MNRAS*, 457, 3678, doi: [10.1093/mnras/stw238](https://doi.org/10.1093/mnras/stw238)
- Povich, M. S., Stone, J. M., Churchwell, E., et al. 2007, *ApJ*, 660, 346, doi: [10.1086/513073](https://doi.org/10.1086/513073)
- Querejeta, M., Schinnerer, E., Meidt, S., et al. 2021, *A&A*, 656, A133, doi: [10.1051/0004-6361/202140695](https://doi.org/10.1051/0004-6361/202140695)
- Sandstrom, K., et al. subm., *ApJL*
- Sandstrom, K. M., Bolatto, A. D., Draine, B. T., Bot, C., & Stanimirović, S. 2010, *ApJ*, 715, 701, doi: [10.1088/0004-637X/715/2/701](https://doi.org/10.1088/0004-637X/715/2/701)
- Santoro, F., Kreckel, K., Belfiore, F., et al. 2022, *A&A*, 658, A188, doi: [10.1051/0004-6361/202141907](https://doi.org/10.1051/0004-6361/202141907)
- Seok, J. Y., Hirashita, H., & Asano, R. S. 2014, *MNRAS*, 439, 2186, doi: [10.1093/mnras/stu120](https://doi.org/10.1093/mnras/stu120)
- Shaya, E. J., Tully, R. B., Hoffman, Y., & Pomarède, D. 2017, *ApJ*, 850, 207, doi: [10.3847/1538-4357/aa9525](https://doi.org/10.3847/1538-4357/aa9525)
- Smith, J. D. T., Draine, B. T., Dale, D. A., et al. 2007, *ApJ*, 656, 770, doi: [10.1086/510549](https://doi.org/10.1086/510549)
- Thilker, D. A., Braun, R., & Walterbos, R. A. M. 2000, *AJ*, 120, 3070, doi: [10.1086/316852](https://doi.org/10.1086/316852)
- Tielens, A. G. G. M. 2008, *ARA&A*, 46, 289, doi: [10.1146/annurev.astro.46.060407.145211](https://doi.org/10.1146/annurev.astro.46.060407.145211)
- Whitcomb, C. M., Sandstrom, K., Murphy, E. J., & Linden, S. 2020, *ApJ*, 901, 47, doi: [10.3847/1538-4357/abaef6](https://doi.org/10.3847/1538-4357/abaef6)
- Wiebe, D. S., Egorov, O. V., & Lozinskaya, T. A. 2011, *Astronomy Reports*, 55, 585, doi: [10.1134/S1063772911070080](https://doi.org/10.1134/S1063772911070080)
- Wiebe, D. S., Khramtsova, M. S., Egorov, O. V., & Lozinskaya, T. A. 2014, *Astronomy Letters*, 40, 278, doi: [10.1134/S1063773714050065](https://doi.org/10.1134/S1063773714050065)
- Wisnioski, E., Glazebrook, K., Blake, C., et al. 2012, *MNRAS*, 422, 3339, doi: [10.1111/j.1365-2966.2012.20850.x](https://doi.org/10.1111/j.1365-2966.2012.20850.x)

All Authors and Affiliations

OLEG V. EGOROV ¹ KATHRYN KRECKEL ¹ KARIN M. SANDSTROM ² ADAM K. LEROY ³ SIMON C. O. GLOVER ⁴
BRENT GROVES ⁵ J. M. DIEDERIK KRUIJSSEN ⁶ ASHLEY. T. BARNES ⁷ FRANCESCO BELFIORE ⁸ F. BIGIEL ⁷
GUILLERMO A. BLANC ^{9,10} MÉDÉRIC BOQUIEN ¹¹ YIXIAN CAO ¹² JÉRÉMY CHASTENET ¹³
MÉLANIE CHEVANCE ^{4,6} ENRICO CONGIU ¹⁰ DANIEL A. DALE ¹⁴ ERIC EMMELM ^{15,16} KATHRYN GRASHA ¹⁷
RALF S. KLESSEN ^{4,18} KIRSTEN L. LARSON ¹⁹ DAIZHONG LIU ¹² ERIC J. MURPHY ²⁰ HSI-AN PAN ²¹
ISMAEL PESSA ²² JÉRÔME PETY ^{23,24} ERIK ROSOLOWSKY ²⁵ FABIAN SCHEUERMANN ¹ EVA SCHINNERER ²²
JESSICA SUTTER ^{2,26} DAVID A. THILKER ²⁷ ELIZABETH J. WATKINS ¹ AND THOMAS G. WILLIAMS ^{28,22}

¹ *Astronomisches Rechen-Institut, Zentrum für Astronomie der Universität Heidelberg, Mönchhofstraße 12-14, D-69120 Heidelberg, Germany*

² *Center for Astrophysics & Space Sciences, Department of Physics, University of California, San Diego, 9500 Gilman Drive, San Diego, CA 92093, USA*

³ *Department of Astronomy, The Ohio State University, 140 West 18th Avenue, Columbus, Ohio 43210, USA*

⁴ *Universität Heidelberg, Zentrum für Astronomie, Institut für Theoretische Astrophysik, Albert-Ueberle-Str 2, D-69120 Heidelberg, Germany*

⁵ *International Centre for Radio Astronomy Research, University of Western Australia, 35 Stirling Highway, Crawley, WA 6009, Australia*

⁶ *Cosmic Origins Of Life (COOL) Research DAO, coolresearch.io*

⁷ *Argelander-Institut für Astronomie, Universität Bonn, Auf dem Hügel 71, 53121 Bonn, Germany*

⁸ *INAF – Osservatorio Astrofisico di Arcetri, Largo E. Fermi 5, I-50157, Florence, Italy*

⁹ *Observatories of the Carnegie Institution for Science, 813 Santa Barbara Street, Pasadena, CA 91101, USA*

¹⁰ *Departamento de Astronomía, Universidad de Chile, Camino del Observatorio 1515, Las Condes, Santiago, Chile*

¹¹ *Centro de Astronomía (CITEVA), Universidad de Antofagasta, Avenida Angamos 601, Antofagasta, Chile*

¹² *Max-Planck-Institut für extraterrestrische Physik, Giessenbachstraße 1, D-85748 Garching, Germany*

¹³ *Sterrenkundig Observatorium, Universiteit Gent, Krijgslaan 281 S9, B-9000 Gent, Belgium*

¹⁴ *Department of Physics and Astronomy, University of Wyoming, Laramie, WY 82071, USA*

¹⁵ *European Southern Observatory, Karl-Schwarzschild Straße 2, D-85748 Garching bei München, Germany*

¹⁶ *Univ Lyon, Univ Lyon 1, ENS de Lyon, CNRS, Centre de Recherche Astrophysique de Lyon UMR5574, F-69230 Saint-Genis-Laval, France*

¹⁷ *Research School of Astronomy and Astrophysics, Australian National University, Canberra, ACT 2611, Australia*

¹⁸ *Universität Heidelberg, Interdisziplinäres Zentrum für Wissenschaftliches Rechnen, Im Neuenheimer Feld 205, D-69120 Heidelberg, Germany*

¹⁹ *AURA for the European Space Agency (ESA), Space Telescope Science Institute, 3700 San Martin Drive, Baltimore, MD 21218, USA*

²⁰ *National Radio Astronomy Observatory, 520 Edgemont Road, Charlottesville, VA 22903-2475, USA*

²¹ *Department of Physics, Tamkang University, No.151, Yingzhuang Rd., Tamsui Dist., New Taipei City 251301, Taiwan*

²² *Max-Planck-Institut für Astronomie, Königstuhl 17, D-69117, Heidelberg, Germany*

²³ *Institut de Radioastronomie Millimétrique (IRAM), 300 Rue de la Piscine, F-38406 Saint Martin d'Hères, France*

²⁴ *LERMA, Observatoire de Paris, PSL Research University, CNRS, Sorbonne Universités, 75014 Paris*

²⁵ *Department of Physics, University of Alberta, Edmonton, AB T6G 2E1, Canada*

²⁶ *Leibniz-Institut für Astrophysik Potsdam (AIP), An der Sternwarte 16, 14482 Potsdam, Germany*

²⁷ *Department of Physics and Astronomy, The Johns Hopkins University, Baltimore, MD 21218, USA*

²⁸ *Sub-department of Astrophysics, Department of Physics, University of Oxford, Keble Road, Oxford OX1 3RH, UK*